



**HAL**  
open science

## Lensfree diffractive tomography for the imaging of 3D cell cultures

Anthony Berdeu, Fabien Momey, Jean-Marc Dinten, Xavier Gidrol, Nathalie Picollet-d'Hahan, Cédric Allier

► **To cite this version:**

Anthony Berdeu, Fabien Momey, Jean-Marc Dinten, Xavier Gidrol, Nathalie Picollet-d'Hahan, et al.. Lensfree diffractive tomography for the imaging of 3D cell cultures. SPIE BiOS, Jan 2017, San Francisco, United States. pp.1007008, 10.1117/12.2250152 . hal-02268652

**HAL Id: hal-02268652**

**<https://hal.science/hal-02268652>**

Submitted on 21 Aug 2019

**HAL** is a multi-disciplinary open access archive for the deposit and dissemination of scientific research documents, whether they are published or not. The documents may come from teaching and research institutions in France or abroad, or from public or private research centers.

L'archive ouverte pluridisciplinaire **HAL**, est destinée au dépôt et à la diffusion de documents scientifiques de niveau recherche, publiés ou non, émanant des établissements d'enseignement et de recherche français ou étrangers, des laboratoires publics ou privés.

# 3D lens-free microscopy for 3D cell culture

Anthony Berdeu<sup>a,b</sup>, Fabien Momey<sup>c</sup>, Jean-Marc Dinten<sup>a,b</sup>, Xavier Gidrol<sup>a,d,e</sup>, Nathalie Picollet-D’hahan<sup>a,d,e</sup>, and Cédric Allier<sup>a,b</sup>

<sup>a</sup>Univ. Grenoble Alpes, F-38000 Grenoble, France

<sup>b</sup>CEA, LETI, MINATEC Campus, F-38054 Grenoble, France

<sup>c</sup>Laboratoire Hubert Curien - Univ. Jean Monnet, F-42100 Saint-Étienne, France

<sup>d</sup>CEA, BIG, Biologie à Grande Echelle, F-38054 Grenoble, France

<sup>e</sup>INSERM, U1038, F-38054 Grenoble, France

## ABSTRACT

New microscopes are needed to help reaching the full potential of 3D organoid culture studies by gathering large quantitative and systematic data over extended periods of time while preserving the integrity of the living sample. In order to reconstruct large volumes while preserving the ability to catch every single cell, we propose new imaging platforms based on lens-free microscopy, a technic which is addressing these needs in the context of 2D cell culture, providing label-free and non-phototoxic acquisition of large datasets. We built lens-free diffractive tomography setups performing multi-angle acquisitions of 3D organoid cultures embedded in Matrigel<sup>TM</sup> and developed dedicated 3D holographic reconstruction algorithms based on the Fourier diffraction theorem. Nonetheless, holographic setups do not record the phase of the incident wave front and the biological samples in Petri dish strongly limit the angular coverage. These limitations introduce numerous artefacts in the sample reconstruction. We developed several methods to overcome them, such as multi-wavelength imaging or iterative phase retrieval. The most promising technic currently developed is based on a regularised inverse problem approach directly applied on the 3D volume to reconstruct. 3D reconstructions were performed on several complex samples such as 3D networks or spheroids embedded in capsules with large reconstructed volumes up to  $\sim 25 \text{ mm}^3$  while still being able to identify single cells. To our knowledge, this is the first time that such an inverse problem approach is implemented in the context of lens-free diffractive tomography enabling to reconstruct large fully 3D volumes of unstained biological samples.

**Keywords:** Diffractive optics, Digital holography, Image reconstruction techniques, Imaging systems, Three-dimensional microscopy.

## 1. INTRODUCTION

The study of in vitro cell populations remains a challenging task if one needs to gather large quantitative and systematic data over extended periods of time while preserving the integrity of the living sample. As discussed in Ref. 1, there is a need for a new microscopy technique that must be label-free and non-phototoxic to be as 'gentle' as possible with the sample, and 'smart' enough to observe the sample exhaustively at a variety of scales both in space and time. Lens-free video microscopy is addressing these needs in the context of 2D cell culture.<sup>2,3</sup>

As scientists better understand the benefit of growing organoids in 3D and routinely adopt 3D culture techniques, lens-free imaging must also be adapted to 3D cultures. Therefore, the new challenging task is to extend lens-free microscopy techniques to the acquisitions and fully 3D reconstructions of large organoids structures.<sup>4-6</sup> The adaptation of lensless microscopy techniques to 3D organoid cultures imaging is the scope of the present paper.

---

Further author information: (Send correspondence to Anthony Berdeu and Fabien Momey)

Anthony Berdeu: anthony.berdeu@cea.fr

Fabien Momey: fabien.momey@univ-st-etienne.fr

Co-corresponding authors: Nathalie Picollet-D’hahan and Cédric Allier

We first describe an experimental bench dedicated to lens-free diffractive tomography of 3D biological samples. Next, we present the Fourier diffraction theorem and the three dedicated reconstruction algorithms we developed to retrieve 3D objects. We conclude with 3D reconstructions of a HUVEC cell culture and a RWPE1 prostatic cell culture grown in 3D to compare the performances of the three proposed reconstruction methods.

## 2. MATERIALS AND METHODS

### 2.1 Experimental bench

Unlike 2D lens-free imaging, where only one image is needed for retrieving the 2D sample, the reconstruction of a 3D object from lens-free acquisitions requires to multiply the viewing angles. For this purpose, we have developed an experimental bench, illustrated in Fig.1. It is composed of a semi-coherent *RGB* illumination source\* and CMOS sensor†.

The experimental bench follows the traditional pattern of the 2D lens-free microscopy (see Fig. 1). The object is placed in between a sensor and a semi-coherent illumination. Nonetheless, the illumination is tilted by an angle of  $\theta = 45^\circ$  and the sensor is slightly deported so that the geometrical projection of the 3D object of interest remains centered regardless of angle  $\varphi$  around the sample. This allows to optimise the the field of view, increasing the overall volume that one can reconstruct.

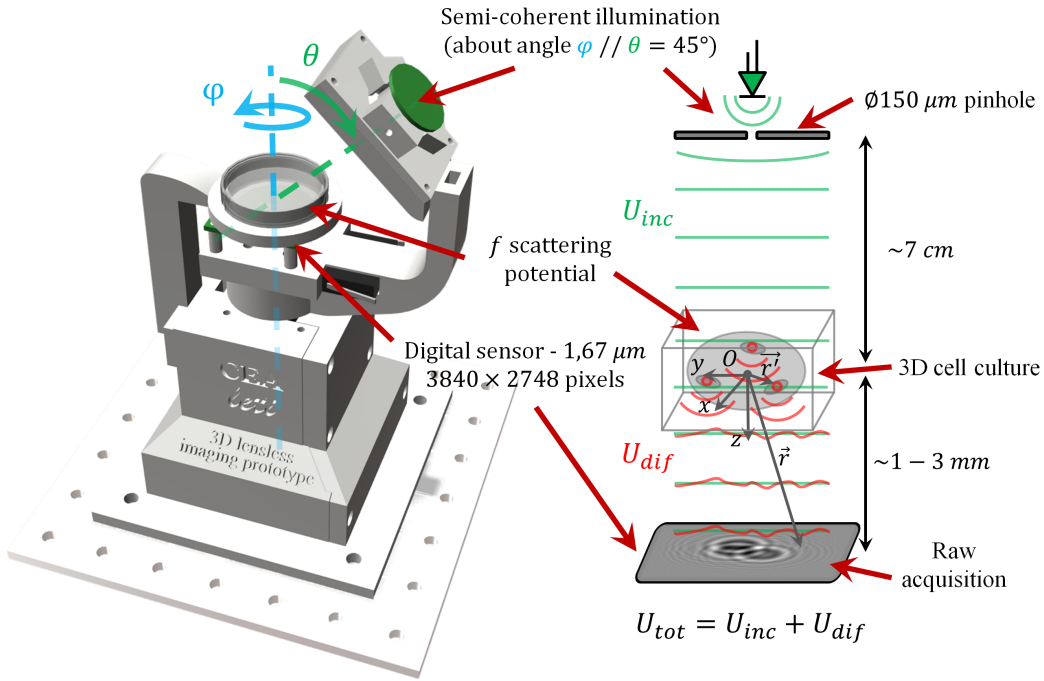


Figure 1. *Left-hand side* - Experimental bench dedicated to lens-free diffractive tomography. *Right-hand side* - Optical scheme of the system. The semi-coherent incident plane wave  $U_{inc}$  is scattered by the 3D sample: each element of the volume behaves like a secondary spherical source, creating a diffracted wave  $U_{dif}$ . The sensor records the intensity of their summation:  $I_{tot} = |U_{tot}|^2$  with  $U_{tot} = U_{inc} + U_{dif}$

### 2.2 Fourier diffraction theorem

It is possible to show<sup>7</sup> that it exists a strong link between the diffracted wave  $U_{dif}$  and the scattering potential  $f$  of the 3D object to reconstruct:

$$f(\vec{r}) = \left( \left( \frac{n(\vec{r})}{n_0} \right)^2 - 1 \right) \quad (1)$$

\*LED CREE,  $\lambda \in \{450, 520, 630 \text{ nm}\}$  - ref. XLamp MC-E RGBW MCE4CT

†CMOS sensor - IDS -  $29.4 \text{ mm}^2$ ,  $3840 \times 2748$  monochromatic pixels, pixel pitch  $1.67 \text{ micrometers}$  - ref. UI-1942LE-M

This is the Fourier diffraction theorem which states that, at a given plane  $z = z_s$  and for an incident plane wave  $U_{inc}(\vec{r}) = e^{i\vec{k}_0 \cdot \vec{r}}$  in a medium of refractive index  $n_0$ , the 2D Fourier transform of  $U_{dif}$  and the 3D Fourier transform of  $f$  are linked by the relation (using the notation of Fig. 2):

$$\hat{f}(\alpha, \beta, \gamma) = \frac{4\pi}{ik_0^2} w e^{-2i\pi w z_s} \hat{U}_{dif}(u, v; z_s) \quad (2)$$

where  $(u, v)$  and  $(\alpha, \beta, \gamma)$  are respectively the coordinates in the Fourier space<sup>‡</sup> on the plane  $z = z_s$  and in the Fourier space of the object which satisfy the following relations:

$$\begin{cases} \alpha = u - u_0 \\ \beta = v - v_0 \\ \gamma = w - w_0 \end{cases} \quad \text{and } w(u, v) = \sqrt{\frac{n_0^2}{\lambda^2} - u^2 - v^2} \quad (3)$$

with  $(u_0, v_0, w_0) = \frac{n_0}{\lambda} (p_0, q_0, m_0)$ .

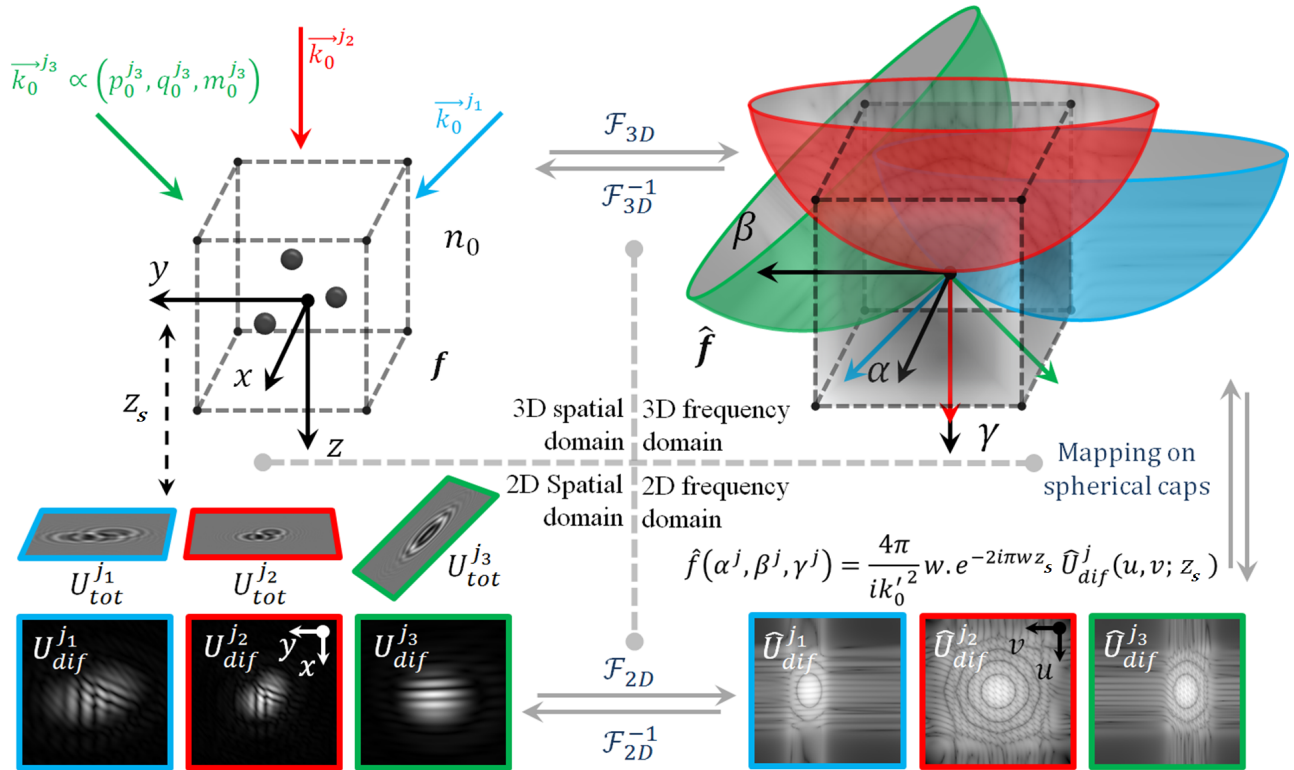


Figure 2. Illustration of the geometrical interpretation of the Fourier diffraction theorem. A 3D Fourier transform links the 3D spatial and frequency domains of the scattering potential  $f$ . A 2D Fourier transform links the 2D spatial and frequency domains of the diffracted wave  $U_{dif}$  for each lighting situation  $j$ . A mapping on spherical caps links the 2D frequency domain of the diffracted wave and the 3D frequency domain of the object. The orientation and position of these caps directly depend on the lighting direction  $\vec{k}_0^j \propto (p_0^j, q_0^j, m_0^j)$ .

Let's note here that, looking more closely at Fig. 2, this theorem can be used both for simulation purposes (going clockwise on the figure from a 3D simulated object to the diffracted waves  $U_{dif}$  in terms of the lighting positions) or for direct reconstruction (going counter-clockwise on the figure from the diffracted waves recorded by the sensor toward the retrieved object via a mapping of the Fourier domain on spherical caps).

<sup>‡</sup>Note that the Fourier transform and its inverse transform are defined for a given function  $g$  as:  $\mathcal{F}(g)(u) = \hat{g}(u) = \int_{-\infty}^{\infty} g(x) e^{-2i\pi ux} dx$  and  $\mathcal{F}^{-1}(\hat{g})(x) = \int_{-\infty}^{\infty} \hat{g}(u) e^{2i\pi ux} du$ . This definition extends naturally to higher dimensions.

Let's also mention that this theorem requires knowledge of the diffracted wave  $U_{dif}$  both in amplitude and phase, whereas with our setup only  $I_{tot} = |U_{tot}|^2$  is recorded by the sensor. Hence there is a lack of phase information in the hologram space as this is the case in 2D lensfree microscopy.

### 2.3 Reconstruction methods

The first step of each methods is a registration of the data: a region of interest is chosen in the dataset and the different frames at different angles are aligned on this pattern via a Least Squares minimisation algorithm, as described in Ref. 6.

Once the data are aligned on specific holograms recorded at different angles, three different methods were developed to reconstruct 3D samples from the 2D acquisitions.

The first two methods are based on the Fourier diffraction theorem used to map the Fourier domain  $\hat{f}$  of the 3D object  $f$ . Each acquisition with a different illumination gives information on coefficients of  $\hat{f}$  lying on spherical caps (Fig. 2 used counter-clockwise). Both methods require an estimation of the diffracted wave  $U_{dif}$ .

**Phase ramp** In this method (see Ref. 6) the unknown phase on the sensor is estimated as being a phase ramp, whose characteristics match the ones of the illumination. This method has the advantage to be fast, allowing to reconstruct large volumes in a small amount of time. Nevertheless, one can note that on the one hand, this remains a strong approximation on the phase and on the other hand, only a small part of the Fourier domain of the object is accessible: the coefficients on which lie the spherical caps. One can expect strong artefacts.

**Phase retrieval** In this method, the unknown phase on the sensor is estimated by an iterative phase retrieval on each 2D pictures of the dataset: the 3D object is approximated by an average median plan and standard algorithm of phase retrieval developed in the realm of 2D lens-free imaging can be applied. This method solves one pitfall of the previous one: the phase introduced in the reconstruction is more realistic and can reduce some artefacts. Nevertheless, it does not solve the problem of the Fourier mapping limitations: only the same coefficients on the spherical caps are accessible.

**3D inverse problem** The last method presented here uses the Fourier diffraction theorem as a direct model for simulating the data, *i.e.* the recorded intensity of the total wave  $U_{tot}$  (Fig. 2 used clockwise). This model is used to perform an inverse problem approach for iteratively retrieving the 3D object.

$$\tilde{f} = \underset{C(f)}{\operatorname{argmin}} \underbrace{\sum_{\vec{k}_0^j} \left\| I_d^{\vec{k}_0^j} - \left| U_{inc}^{\vec{k}_0^j} + U_{dif}^{\vec{k}_0^j}(f) \right|^2 \right\|^2}_{\text{data fidelity}} + \underbrace{\mu_r \|f\|_r}_{\text{regularisation}} \quad (4)$$

The first advantage of such an approach is that we are able to model the end-to-end non-linear process of data acquisition and to solve the inverse problem without requiring a direct inversion of the model by comparing the experimental data  $I_d^{\vec{k}_0^j}$  for a given illumination  $k_0^j$  with the simulated data  $\left| U_{inc}^{\vec{k}_0^j} + U_{dif}^{\vec{k}_0^j}(f) \right|^2$  for a given scattering potential  $f$ . The second advantage is that one can add a priori information to the reconstruction process such as possible constraints on the definition domain  $C(f)$  or via a regularisation term  $\mu_r \|f\|_r$ . In this work, we tested two kinds of regularised norms: the  $L_1$ -norm, fostering sparse reconstruction, and the total variation, a constraint on the sparsity of the image gradient, leading to sharp objects. This method also allows to improve the alignment of the data among the iterations, increasing the overall reconstruction quality. Indeed, one can use the simulated data as a reference to better align the experimental data set.

Compared with the two previous methods, this solution is extremely time consuming but it solves the raised problems: a phase is estimated via the inverse problem approach and the whole Fourier domain is used in the reconstruction if an adequate regularisation is applied.

### 3. EXPERIMENTAL RESULTS

#### 3.1 On HUVEC network

Fig. 3 presents a comparison of the methods on a HUVEC network. These are Human Umbilical Vein Endothelial Cells which tend to create networks when they are seeded on an extracellular matrix bed. The dataset is composed of  $3 \times 16$  acquisitions done at 16 different angles ( $\Delta\varphi = 18.8^\circ$ ) in the three available wavelengths of the LED.

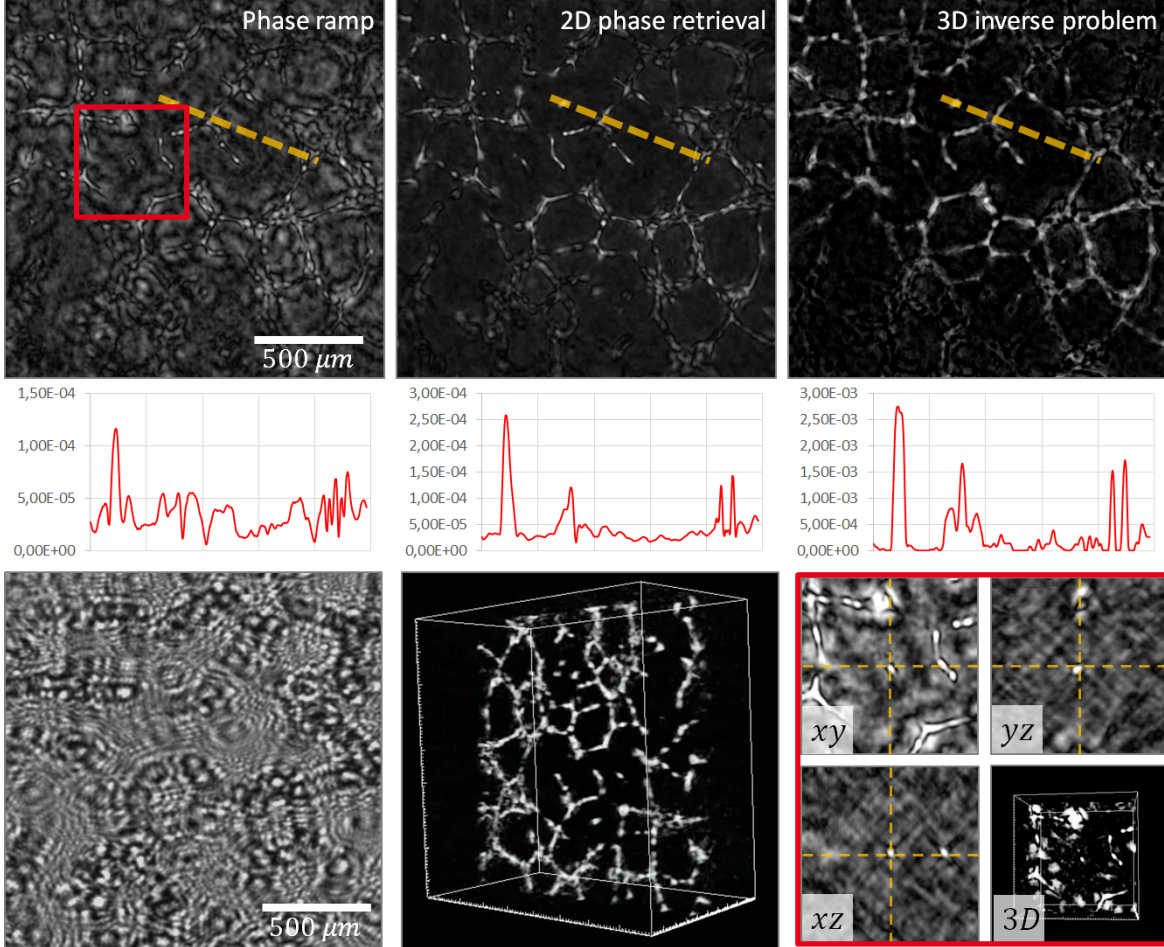


Figure 3. Comparison of the reconstruction methods on a HUVEC network. The cells spread on the Matrigel<sup>TM</sup> surface and the final network is overall planar. The profiles correspond to the yellow dashed-lines. The red framed zoom in the lower right corner emphasizes the artefacts of reconstruction with the phase ramp approximation around an isolated cell. The lower left corner presents a data acquisition in the red channel next to a 3D view of the reconstructed volume. Reconstruction parameters:  $\varphi \in \{0^\circ, 282^\circ\}$ ,  $\Delta\varphi = 18.8^\circ$ ,  $\theta = 45^\circ$ ,  $\lambda_0 = RGB$ ,  $z_s = 3.3 \text{ mm}$ ,  $512 \times 512 \times 300$  voxels of  $3.34 \times 5.32 \mu\text{m}^3$ . Final volume:  $1.7 \times 1.7 \times 1.6 \text{ mm}^3 = 4.7 \text{ mm}^3$ .

The zoom in the red medallion shows the artefacts of the first method around an isolated single cell: on the  $xy$ -plane one can see white and black residues around the branches. These are twin-images of the focused object, a well-known phenomenon in classical 2D in-line holography due to the lack of phase information. On the  $xz/yz$ -plane, some artefacts on straight lines due to the limited angular coverage are visible. Nonetheless, the object has a similar spatial extension in the three directions.

As one can expect, the twin-image artefacts is strongly reduced as soon as a 2D phase retrieval is performed. Orthogonal views (not presented here) on the 3D reconstruction performed with the 2D phase retrieval method

would show nevertheless that the second type of artefacts due to the limited angular views are still present. They tend to disappear in the reconstruction done with a 3D inverse problem approach.

Looking at the profiles, one can see that the signal-to-noise ratio (SNR), empirically defined here as the ratio of the intensity of the objects compared to the mean background value, increases between the two first methods thanks to the diminution of the twin-image signal and the signal of isolated cell gains a factor 10 with the inverse problem approach. On such data, one can wonder if using a 3D inverse problem is the best solution: indeed, the 2D phase retrieval method appear to be enough to analyse the network structures and is obtained with a faster running code (see table 1).

### 3.2 On RWPE1 prostatic cells

Fig. 4 presents similar views on a prostatic cell culture embedded in Matrigel<sup>TM</sup>. They tend to create organoids. Once they are stabilized, they start to grow networks. The field of view appears more crowded than in the previous section and the sample presents a 3D spatial extension. The dataset is composed of  $3 \times 16$  acquisitions done at 16 different angles ( $\Delta\varphi = 18.8^\circ$ ) in the three available wavelengths of the LED.

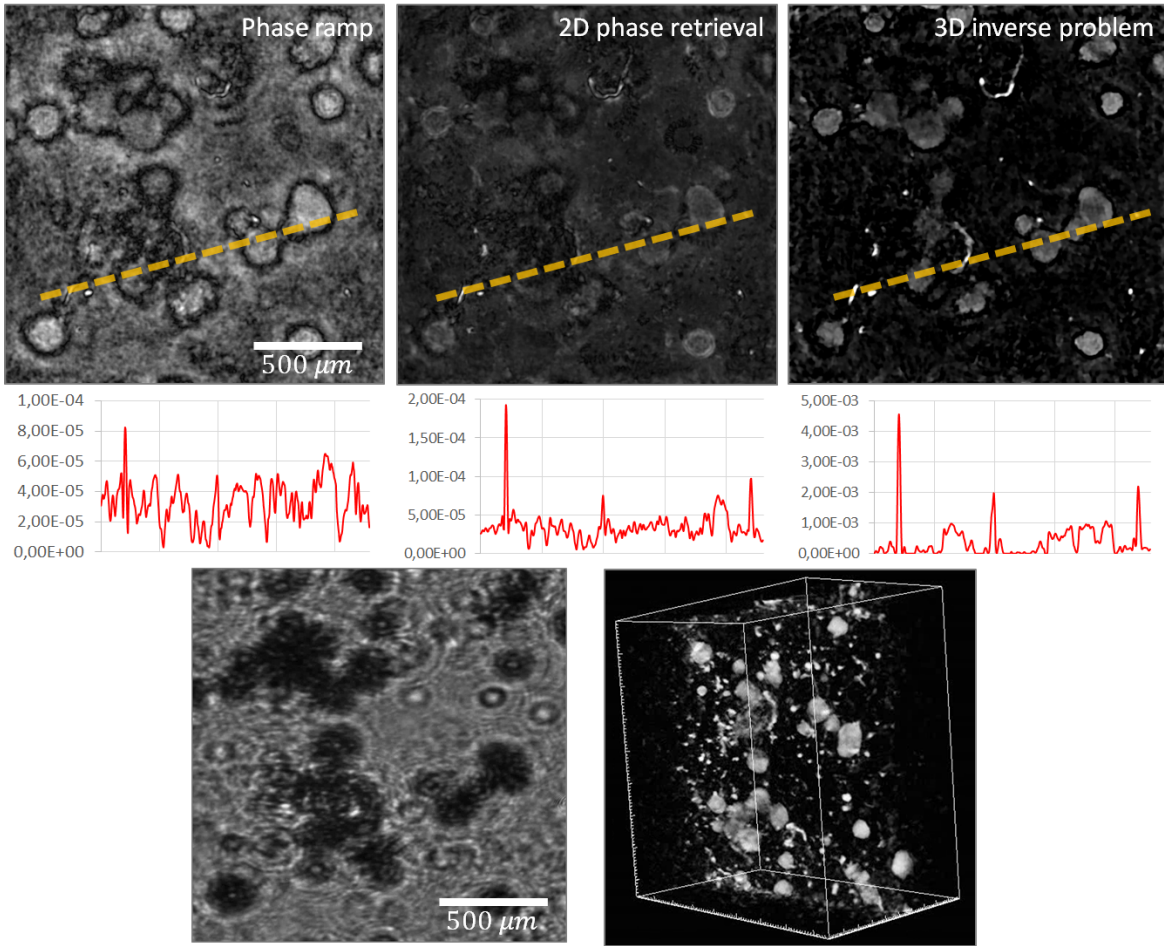


Figure 4. Comparison of the reconstruction methods on a RWPE1 network. The cells tend to form organoids when embedded in Matrigel<sup>TM</sup>. The profiles correspond to the yellow dashed-lines. The lower left corner presents a data acquisition in the red channel. Reconstruction parameters:  $\varphi \in \{0^\circ, 282^\circ\}$ ,  $\Delta\varphi = 18.8^\circ$ ,  $\theta = 45^\circ$ ,  $\lambda_0 = RGB$ ,  $z_s = 3.3 \text{ mm}$ ,  $512 \times 512 \times 300$  voxels of  $3.34 \times 5.32 \mu\text{m}^3$ . Final volume:  $1.7 \times 1.7 \times 1.6 \text{ mm}^3 = 4.7 \text{ mm}^3$ .

Similar conclusions can be obtained concerning the artefacts and the augmentation of the SNR. But furthermore, the 3D inverse problem approach shows here its advantages over the two other methods: the organoids

are sharper and well localized. Some are even not visible with the two other methods. It gives credit to this method, despite its long computational time which can appear as prohibitory (see table 1).

Table 1. Comparison of the reconstruction times with the different method. They were obtained with our Matlab<sup>TM</sup> code running on a Intel(R) Xeon(R) CPU E5-2620 v3 @ 2.40 GHz processor. The code was not designed to be optimised and the given times can only be considered as an order of magnitude for comparison purposes.

	Phase ramp	2D phase retrieval	3D inverse problem
HUVEC	$\sim 1 \text{ min}$	$\sim 16 \times 5 + 2 \text{ min}$	$\sim 7 \text{ h}$
RWPE1	$\sim 1 \text{ min}$	$\sim 16 \times 7 + 2 \text{ min}$	$\sim 10 \text{ h}$

## 4. CONCLUSION

We presented a novel tool to perform acquisition on large 3D cell cultures. Based on the in-line holographic principle, it can image unlabelled and unstained samples. To overcome the limitations raised by such a microscope, that is to say the lack of phase and the limited angular coverage, we developed three dedicated algorithms.

We showed that these algorithms are able to retrieve the 3D object but with different qualities in terms of signal-over-noise ratio and computational time. Giving the result in a single pass, the algorithm based on a phase ramp is fast but leads to a signal which can be hard to distinguish from the artefacts and the noise. Providing the best SNR, the algorithm based on the 3D inverse problem approach can nevertheless be extremely time consuming.

It appears then that the choice to use either an algorithm or another will depend on the targeted application. To identify isolated single cells in a 3D volume, which provide a strong signal, the first algorithm can be sufficient. On the other hand if one aims at reconstructing complex overlapping structures, only the 3D regularised iterative reconstruction can provide a pertinent result.

## ACKNOWLEDGMENTS

We would like to thank Thomas Bordy for his great help for the device conception both for the electronics and the software. And we are grateful to Fabrice Navaro, Stéphanie Porte and Bastien Laperrousaz who provided the biological cultures.

## REFERENCES

- [1] Scherf, N. and J. Huisken, J., “The smart and gentle microscope,” *Nature Biotechnology* (2015).
- [2] Kesavan, S. V., Momey, M., Cioni, O., David-Watine, B., Dubrulle, N., Shorte, S., Sulpice, E., Freida, D., Chalmond, B., Dinten, J. M., Gidrol, X., and Allier, C., “High-throughput monitoring of major cell functions by means of lensfree video microscopy,” *Scientific Reports* **4** (Aug. 2014).
- [3] Zheng, Z., Lee, S. A., Antebi, Y., Elowitz, M. B., and Yang, C., “The ePetri dish, an on-chip cell imaging platform based on subpixel perspective sweeping microscopy (SPSM),” *Proceedings of the National Academy of Sciences, U.S.A* **108**(18), 16889–16894 (2011).
- [4] Dolega, M. E., Allier, C., Kesavan, S. V., Gerbaud, S., Kermarrec, F., Marcoux, P., Dinten, J.-M., Gidrol, X., and Picollet-D’Hahan, N., “Label-free analysis of prostate acini-like 3d structures by lensfree imaging,” *Biosensors and Bioelectronics* **49**, 176 – 183 (2013).
- [5] Isikman, S. O., Bishara, W., Mavandadi, S., Yu, F. W., Feng, S., Lau, R., and Ozcan, A., “Lens-free optical tomographic microscope with a large imaging volume on a chip,” *Proceedings of the National Academy of Sciences* **108**(18), 7296–7301 (2011).
- [6] Momey, F., Berdeu, A., Bordy, T., Dinten, J.-M., Marcel, F. K., Picollet-D’hahan, N., Gidrol, X., and Allier, C., “Lensfree diffractive tomography for the imaging of 3D cell cultures,” *Biomedical Optics Express* **7**, 949–962 (Mar 2016).
- [7] Wolf, E., “Three-dimensional structure determination of semi-transparent objects from holographic data,” *Optics Communications* (1969).